

Symmetrized density matrix renormalization group algorithm for low-lying excited states of conjugated carbon systems: Application to 1,12-benzoperylene and polychrysene

Suryoday Proadhan* and S. Ramasesha†

Solid State and Structural Chemistry Unit, Indian Institute of Science, Bangalore-560012, India

(Received 15 October 2017; revised manuscript received 14 April 2018; published 14 May 2018)

The symmetry adapted density matrix renormalization group (SDMRG) technique has been an efficient method for studying low-lying eigenstates in one- and quasi-one-dimensional electronic systems. However, the SDMRG method had bottlenecks involving the construction of linearly independent symmetry adapted basis states as the symmetry matrices in the DMRG basis were not sparse. We have developed a modified algorithm to overcome this bottleneck. The new method incorporates end-to-end interchange symmetry (C_2), electron-hole symmetry (J), and parity or spin-flip symmetry (P) in these calculations. The one-to-one correspondence between direct-product basis states in the DMRG Hilbert space for these symmetry operations renders the symmetry matrices in the new basis with maximum sparseness, just one nonzero matrix element per row. Using methods similar to those employed in the exact diagonalization technique for Pariser-Parr-Pople (PPP) models, developed in the 1980s, it is possible to construct orthogonal SDMRG basis states while bypassing the slow step of the Gram-Schmidt orthonormalization procedure. The method together with the PPP model which incorporates long-range electronic correlations is employed to study the correlated excited-state spectra of 1,12-benzoperylene and a narrow mixed graphene nanoribbon with a chrysene molecule as the building unit, comprising both zigzag and cove-edge structures.

DOI: [10.1103/PhysRevB.97.195125](https://doi.org/10.1103/PhysRevB.97.195125)

I. INTRODUCTION

The density matrix renormalization group method (DMRG), put forward by White [1,2], is a many-body method of choice for studying low-lying states of one- and quasi-one-dimensional π -conjugated models [3–23]. Although the single configuration interaction (SCI) approximation is the conventional approach for deducing an optical gap in quantum chemical calculations, its limitations for many particle-hole states are well documented [24–34]. Employing time-dependent density functional theory [35–37] or the GW approximation accompanied by a Bethe-Salpeter correction [38–40], optical properties of a number of π -conjugated systems have been investigated in the past; however, these methods are equivalent to SCI approximation as only one-electron–one-hole excitations are considered in these calculations. The consequences of two-electron–two-hole and higher excitations, which are necessary for the accurate description of the spectra of strongly correlated systems, are difficult to probe within these methods. Full configuration interaction studies are computationally expensive as the Hilbert-space size grows exponentially with system sizes and are limited to ~ 18 -orbital half-filled systems. In the literature, there are reports of some *ab initio* quantum chemical methods, such as the complete active space second-order perturbation theory, the third-order coupled cluster theory, or the extended algebraic diagrammatic construction method which can correctly reproduce the energy spectra of polyenes, yet, they are limited to very small size

systems [41–45]. The multiple-reference configuration interaction approach is suitable to study higher-order configuration interaction effects accurately, but the Hilbert-space dimensions for different excited states, for similar accuracy, can be significantly different; the calculations are performed iteratively for updating the many-body basis space until convergence is reached [32,33,46].

On the contrary, in the DMRG method because of the renormalization procedure, the Hilbert-space dimension remains fixed independent of the system sizes and can be employed to probe behaviors in the polymer limit. For gapped systems, the area law of entanglement entropy holds leading to high accuracy in the DMRG calculations [47,48] with a moderate cutoff in the number of block states. However, the DMRG method as introduced by White [1,2] is not a symmetry-based method. Conventional DMRG algorithms exploit symmetries, such as conservation of the particle number and the total S_z value of the superblock Hamiltonian [47]. In conjugated systems, the states of interest for optical studies are usually the one-photon and two-photon states. Depending upon the system size and correlation strength, the number of states that intrude between the ground state and the desired states are variable and large. This makes targeting “important” states almost impossible without invoking the basic symmetries, namely, the C_2 (end-to-end interchange) symmetry and the electron-hole symmetry, which exist in half-filled bipartite lattices. Ramasesha and co-workers [49] developed a method to exploit these symmetries in Hamiltonians with long-range interactions in quantum-cell models to target one- and two-photon states. The slow step in the algorithm was the need to orthonormalize the symmetrized basis vectors and eliminate the linear dependencies. The step was also computationally

*suryodayp@iisc.ac.in

†ramasesh@iisc.ac.in

TABLE I. Ground-state energies [$E(1^1A^+)$], lowest optical gaps [$\Delta E(1^1B^-)$], and lowest two-photon gaps [$\Delta E(2^1A^+)$] of PPV oligomers with N monomers, calculated by Bursill and Barford (BB) [18] and by the present symmetrized DMRG algorithm within the noninteracting model are compared against the exact results. All energies and energy gaps are given in units of eV. The BB results are reproduced from Ref. [18] which employs only the infinite DMRG method. In our calculations, we have employed the finite DMRG algorithm with two sweeps. Notably, the differences in energy gaps calculated by the present algorithm from the exact results are quite within the experimental accuracy.

N	$E(1^1A^+)$			$\Delta E(1^1B^-)$			$\Delta E(2^1A^+)$		
	BB [18]	Present algorithm ^a	Exact	BB [18]	Present algorithm ^a	Exact	BB [18]	Present algorithm ^a	Exact
2	-47.6624938	-47.6624937	-47.6624938	2.928370	2.928369	2.928369	4.302947	4.302950	4.302947
3	-75.0319491	-75.0319486	-75.0319491	2.428260	2.428260	2.428259	3.120478	3.120471	3.120467
4	-102.402074	-102.402074	-102.402075	2.213363	2.213378	2.213355	2.671863	2.671874	2.671844
5	-129.772242	-129.772242	-129.772243	2.099678	2.099718	2.099665	2.427314	2.427354	2.427288
6	-157.142411	-157.142413	-157.142414	2.031963	2.032110	2.031921	2.278100	2.278237	2.278027
7	-184.512579	-184.512585	-184.512587	1.988297	1.988481	1.988233	2.180004	2.180146	2.179900
8	-211.882729	-211.882756	-211.882759	1.958526	1.958878	1.958402	2.112045	2.112277	2.111848
9	-239.252894	-239.252928	-239.252938	1.937287	1.937688	1.937126	2.062944	2.063183	2.062696
10	-266.623033	-266.623099	-266.623103	1.921674	1.922290	1.921420	2.026410	2.026738	2.026035
11	-293.993193	-293.993271	-293.993275	1.909792	1.910466	1.909498	1.998400	1.998742	1.997966

^aThe superblock Hilbert-space size in the calculations by BB varies between $\sim 3 \times 10^5$ and 3×10^6 . In our calculations, the superblock Hilbert-space dimension varies between $\sim 5 \times 10^4$ and 1×10^5 .

intensive since the matrices representing the symmetry operators were not sparse. A modification was introduced by Bursill and co-workers in the algorithm to study relevant low-lying eigenstates, primarily in *trans*-polyacetylene [8–10,14,15,19], polydiacetylene [16,17], poly(para-phenylene) [6,11,13], and poly(para-phenylene vinylene) [6,7,12,18], which leads to sparseness in the symmetry operator matrices and generates one-to-one symmetry correspondence between different direct product basis states [18,19]. Their method is based on the assumption that all symmetry operators (as defined in Ref. [49]) are their own inverse in every basis space, which, although true for spin-flip or parity symmetry, is not true for electron-hole symmetry. They developed the formalism explicitly for a single symmetry, and they wrongly hypothesized that the same will apply when more symmetries are present. Within this formalism, they assumed that the relevant density matrix eigenstates (block states) are nondegenerate. As a consequence, each block state is an eigenvector of the block symmetry operators with eigenvalue ± 1 . They argued that block states with degenerate reduced density matrix eigenvalues, although not exact eigenstates of the block symmetry operator, usually have low weight in the target eigenstate of the full system. Hence, an approximation to their block symmetry eigenvalues, taken as $+1$ if the expectation value for the corresponding symmetry operator is positive and -1 if it is negative, is made [18]. Although, this scheme has been adequate for linear systems, such as *trans*-polyacetylene and polydiacetylene, or simple quasi-one-dimensional systems, such as poly(para-phenylene) and poly(para-phenylene vinylene), the important block states become degenerate for complex systems, such as fused conjugated molecules (nanoribbons and nanoflakes) and quasi-two-dimensional systems. They also incorrectly assumed that all symmetry operators in a block commute with each other. In this paper, we explicitly describe how the above-mentioned symmetries of a system can be employed systematically going beyond the approximate treatment of Bursill and Barford (BB) [18]. This modified symmetrization

scheme has already been successfully employed to probe low-lying excited states in graphene nanoribbons [34] as well as in molecular graphene nanoflakes [50]. We have also compared here our calculations for poly(para-phenylene vinylene) within a noninteracting model with that reported by BB [18] (Table I). We have employed the same parameter set as in Ref. [18] for our calculations. It is indeed difficult to make an accurate comparison with BB as the method used by them replaces phenyl groups by a single virtual site, and although they do not resort to the finite DMRG approach, they do refine the states of the virtual site. The main advantage of our method over that of BB is we treat symmetry adaptation of nearly degenerate block states exactly. This becomes important when the number of block states retained is large, and in this scenario, near (numerical) degeneracy of the retained block states will become significant. We have noted that we have comparable accuracy with that reported in Ref. [18] for a much smaller superblock Hilbert space; this is because the block states in our calculations are exact eigenstates of the block symmetry operators.

In another symmetrized DMRG scheme, utilized mostly in *ab initio* quantum chemical studies [51–53], irreducible representation of a direct product state of the superblock is obtained as a product of the symmetry labels of the respective block states. This scheme is not applicable when working in real space with localized site orbitals as in most of the quantum-cell calculations because the site orbitals do not transform as any irreducible representation of the point group.

In this paper, we have given an account of a highly accurate and efficient DMRG algorithm for utilizing end-to-end interchange symmetry (C_2), electron-hole symmetry (J), and spin-flip or parity symmetry (P). The advantage of this algorithm is that the symmetry operators can be expressed as highly sparse matrices with only one nonzero element per row. This allows for representing the symmetry operators by vectors of the same dimension as the DMRG Hilbert space. Hence, it is possible to employ very large DMRG cutoffs in the new symmetry adaptation algorithm. We have utilized

this new algorithm to calculate the ground state, lowest-lying two-photon and one-photon states along with a few low-lying triplet states in the $S_z = 1$ sector for 1,12-benzoperylene within the long-ranged PPP model. We have also probed the low-lying excited states of a mixed graphene nanoribbon (polychrysene) in the thermodynamic limit within the same long-range interacting model. Similar to our earlier study [34], we have carried out highly accurate finite DMRG calculations on systems of moderate sizes and rely on finite-size scaling to obtain the physical properties in the thermodynamic limit. This system is interesting for two reasons. First, it is a mix of zigzag and cove-edge structures, and to see which edge character dominates in determining the electronic properties will be of interest. Second, the monomer chrysene is closely related to the picene molecule which has reportedly shown superconductivity in alkali-metal complexes [54,55].

Although Abelian symmetries (continuous or discrete) have been introduced in DMRG calculations quite early, characterizing block states with irreducible representations of non-Abelian total spin symmetry [$SU(2)$ symmetry] is tricky. McCulloch and Gulacsi showed that the total spin operator does not commute with the conventional reduced density matrix operator of the system (environment) block but with a quasidensity matrix [56,57]. The quasidensity matrix is obtained from the conventional reduced density matrix by removing matrix elements which mix block states of different spins. Since one- and two-electron operators of the Hamiltonian are generally expressed in the total S_z basis, computationally intensive Clebsch-Gordan (CG) transformations of the operator matrices are required. Later, McCulloch and Gulacsi came up with a modified algorithm [58] where block states are expressed as “spin eigenstates” or “reduced basis states,” labeled only by the total spin value (S). This scheme has been modified further by others [51–53,59], yet, the basic structure has remained same. The block operators are expressed as irreducible tensor operators of rank S with $2S + 1$ components, and the “reduced matrix elements” of the operators get transformed into the S_z basis matrix elements by CG coefficients [60]; a product of two operators from different blocks can be obtained from individual operator matrices using Wigner $9j$ coefficients. However, the overall algorithm becomes computationally expensive owing to the calculation of the CG and Wigner $9j$ coefficients and using them for the transformation of block states and calculation of the superblock Hamiltonian matrix. Alternatively, the spin of a targeted state can be calculated directly from the spin-spin correlation function [61,62]; however, this demands calculation of the spin-spin correlation function for each pair of sites of the superblock. In our present paper, we have avoided using the full spin conservation but have exploited the spin-inversion symmetry of the Hamiltonian instead. The spin-inversion symmetry bifurcates the total Hilbert space with $S_z^{\text{total}} = 0$ into a subspace of odd total spin and a subspace of even total spin. For π -conjugated systems, the ground state usually lies in the even total spin space, and the lowest-energy state in the odd total spin space corresponds to the lowest triplet state of the system. The energy gap between these states constitutes the spin gap of the system.

The paper is organized as follows. In the next section, we have given an account of the modified algorithm. In Sec. III,

we have compared our new results with benchmark exact calculations for 16-site polyene chain and tetracene. In the following sections, we have discussed our results for 1,12-benzoperylene and polychrysene. In the last section we have summarized our study and concluded.

II. MODIFIED ALGORITHM FOR SYMMETRY ADAPTATION

The DMRG procedure is a truncated Hilbert-space algorithm which adopts an iterative block-building scheme for calculating low-lying eigenstates of large one- or quasi-one-dimensional Hamiltonians [1,47]. The system block or left block (L) along with the environment block, also denoted as the right block (R), are linearly grown through the addition of one new site to each block per iteration, and these two together form the superblock which corresponds to the physical system to be studied. In the infinite DMRG algorithm, the superblock of size $2l$ consists of system and environment blocks of same size (l). The reduced density matrix of the system is generated from low-lying eigenstates of the superblock by tracing over the environment states. Matrix elements of the reduced density matrix of the system are represented by $\rho_{m,m'} = \sum_n \psi_{m,n} \psi_{m',n}^*$, where m, m' are system states whereas n 's are the environment states. To construct the reduced density matrix of the right block, the system and environment are interchanged. Reduced density matrices for both the system and the environment are diagonalized, and $M^{(l)}$ density matrix eigenstates or block states with highest eigenvalues ($\{\mu_L\}$ for the system and $\{\mu_R\}$ for the environment) are stored as column vectors of a $M^{(l-1)}d_\sigma \times M^{(l)}$ matrix, where $M^{(l-1)}$ is the number of block states retained at the $(l - 1)$ -th iteration and d_σ is the dimension of the Fock space of the newly added site in the l th iteration. The Hamiltonian and site operators of the newly generated blocks are constructed in the basis $\mu^{(l-1)}\sigma$ and then renormalized using the $M^{(l-1)}d_\sigma \times M^{(l)}$ matrix. Further addition of two new sites gives a system of $2l + 2$ sites, whose basis $|\mu_L^{(l)}\sigma_i\sigma_{i'}\mu_R^{(l)}\rangle$ is generated as a direct product of $|\mu_L^{(l)}\rangle$ of the system block, $|\mu_R^{(l)}\rangle$ of the environment block with $|\sigma_i\rangle$ and $|\sigma_{i'}\rangle$ of the newly added sites to the left and right blocks, respectively. The Hamiltonian for the $2l + 2$ sites system is formed in this direct product space and diagonalized to get the energy eigenstates, which are utilized for the next iteration. In the case of systems with finite-size N , the finite DMRG algorithm enhances the accuracy in the eigenstate calculation; the infinite algorithm is employed starting from a small system until the desired superblock size is reached, and then sweeping over the superblock is applied by changing the system and environment sizes, by one site at each step, keeping the superblock size fixed. The basis at a step of the finite DMRG sweeping can be represented by $|\mu_L^{(l)}\sigma_i\sigma_{i'}\mu_R^{(N-l-2)}\rangle$, where l can vary between 1 and $N - 3$. Once the size of the system (environment) block reaches its maximum, the environment (system) block starts to grow at the expense of the other block. A complete sweep consists of the expansion of both blocks to their maximum and returning to the block size of the final infinite DMRG step.

The symmetry elements considered in our modified algorithm are same as in the work by Ramasesha *et al.* [49]. The

C_2 symmetry about an axis perpendicular to the plane of the molecule corresponds to the end-to-end interchange of the superblock with a phase factor,

$$\hat{C}_2 |\mu_L^{(l)} \sigma_i \sigma_{i'} \mu_R^{(l)}\rangle = (-1)^\gamma |\mu_R^{(l)} \sigma_{i'} \sigma_i \mu_L^{(l)}\rangle,$$

or in shorter notation (which will be used from here on),

$$\hat{C}_2 |\mu \sigma \sigma' \mu'\rangle = (-1)^\gamma |\mu' \sigma' \sigma \mu\rangle,$$

$$\gamma = n_\mu(n_\sigma + n_{\sigma'} + n_{\mu'}) + n_\sigma(n_{\sigma'} + n_{\mu'}) + n_{\sigma'} n_{\mu'},$$

i.e., the system and environment blocks interchange their corresponding block states while the two newly added sites also interchange their Fock states. n_μ , $n_{\mu'}$, n_σ , and $n_{\sigma'}$ are the occupancies in the system block, the environment block, and the two newly added sites. As the interchange should not affect the superblock Hilbert space, the block state spaces corresponding to the system and the environment should be identical. In other words, employing C_2 symmetry approximately halves the effective size of the superblock Hilbert space besides reducing the computational expense by avoiding environment block calculations at every infinite DMRG step and at the last step of the finite DMRG iteration. In this symmetry operation, each direct product basis state is carried over to only one unique direct product basis state with a phase of ± 1 . Thus, the C_2 symmetry operation can be stored as a column vector with entry $\pm j_k$, state j resulting from the C_2 operation on state k , and the \pm sign denoting the phase associated with the C_2 operation.

The Hamiltonian of a half-filled bipartite system conserves electron-hole symmetry (J) where interchanging the creation and annihilation operators at each lattice site with an associated phase factor keeps the Hamiltonian invariant. On application of this symmetry element, Fock states of a single site transform in the following way:

$$\hat{J}_i |\uparrow\rangle = |\downarrow\rangle, \quad \hat{J}_i |\uparrow\rangle = (-1)^{\eta_i} |\uparrow\rangle,$$

$$\hat{J}_i |\uparrow\downarrow\rangle = -|\downarrow\rangle, \quad \hat{J}_i |\downarrow\rangle = (-1)^{\eta_i} |\downarrow\rangle,$$

where η_i is 1 if i belongs to the A sublattice and 0 if it belongs to the B sublattice.

The result of parity or spin-flip symmetry (P) which flips the spin at each site is given by the following:

$$\hat{P}_i |0\rangle = |0\rangle, \quad \hat{P}_i |\uparrow\rangle = |\downarrow\rangle,$$

$$\hat{P}_i |\uparrow\downarrow\rangle = -|\uparrow\downarrow\rangle, \quad \hat{P}_i |\downarrow\rangle = |\uparrow\rangle.$$

Nonrelativistic Hamiltonians remain invariant under parity symmetry. This symmetry can only be employed in $S_z = 0$ space as the application of this symmetry for nonzero S_z maps S_z space to $-S_z$ space.

Both J_i and P_i operators are site operators, and hence, the operators for the full system can be defined as

$$\hat{J} = \prod_i \hat{J}_i, \quad \hat{P} = \prod_i \hat{P}_i.$$

The matrix element of these two symmetry operators for a superblock of size $2l + 2$ can be represented by

$$\langle \mu' \sigma' \sigma \mu | \hat{\mathcal{R}}_{2l+2} | \nu \tau \tau' \nu' \rangle$$

$$= \langle \mu | \hat{\mathcal{R}}_l | \nu \rangle \langle \sigma | \hat{\mathcal{R}}_l | \tau \rangle \langle \sigma' | \hat{\mathcal{R}}_{l'} | \tau' \rangle \langle \mu' | \hat{\mathcal{R}}_l | \nu' \rangle, \quad (1)$$

i.e., it is direct product of matrix elements of corresponding symmetry operators in the block state space of the system block, the block state space of the environment block, and the Fock spaces of the two newly added sites.

The symmetry operators of the superblock follow the relations:

$$(\hat{C}_2)^2 = 1, \quad \hat{J}^2 = (-1)^{N_s + N_e}, \quad \hat{P}^2 = 1, \quad (2)$$

where N_s and N_e are the number of sites and the number of electrons in a basis state on which the symmetry operations are applied. In the case of the half-filled fermionic system $N_s = N_e$; subsequently, each of the operators becomes its own inverse, and the symmetry operators commute among themselves and form an Abelian group. However, the symmetry operators do not commute generally in individual block spaces and in Fock spaces of newly added sites. *This is the fundamental difference of the current algorithm from the one developed by Bursill and co-workers [18,19] since they have incorrectly assumed the involutory nature of the symmetry operators in the block state space resulting in the commutative nature of the block symmetry operators.*

As mentioned earlier, the C_2 symmetry operator maps one direct product state exclusively to another one. However, J and P operators do not produce a single state due to the absence of one-to-one symmetry correspondence between different block states of a particular block, although the mapping of the Fock states of a single site is exclusive. This absence of one-to-one mapping of the block states in system and environment blocks and hence the lack of one-to-one mapping of the direct product states of the superblock leads to some serious problems in symmetry adaptation. First, the matrix representation of the operators in the block state basis is not very sparse. Second, it is difficult to keep track of and thereby include all the symmetry partners of the J and P symmetries while introducing the DMRG cutoff. Third, weeding out linearly dependent states after symmetry adaptation is a slow step as it involves Gram-Schmidt orthonormalization of the symmetrized superblock states. Thus, a successful symmetry adaptation scheme must have a unique one-to-one correspondence between states in the block state space.

We invoke the one-to-one correspondence among different block states which results in only one nonzero element in each row of the matrices of the symmetry operators. This is achieved by considering block states restricted to a specific region of the Hilbert space as by symmetry we can obtain the block states in the complementary spaces. For example, block states with the total number of electrons $n_e < n_s$, the number of sites in the system block, are related to block states with $n_e > n_s$ by

$$\hat{J}_L \mu_i (n_e < n_s) = \mu_j (n_e > n_s), \quad (3)$$

and similarly the block states with $S_z > 0$ are related to block states with $S_z < 0$ by

$$\hat{P}_L \mu_i (S_z < 0) = \mu_j (S_z > 0). \quad (4)$$

Thus, while imposing the truncation procedure of the block state space, we only consider the subspace of block states with $n_e \leq n_s$ and $S_z \leq 0$. Since the block states, resulting from operating on these states by \hat{J} , \hat{P} and $\hat{P}\hat{J}$ will also have the same density matrix eigenvalues, it is ensured that all block states above a cutoff in the density matrix eigenvalue are included.

We now describe our symmetry adaptation procedure that leads to symmetry matrices of the superblock with just one nonzero element in each row (or column) (schematically shown

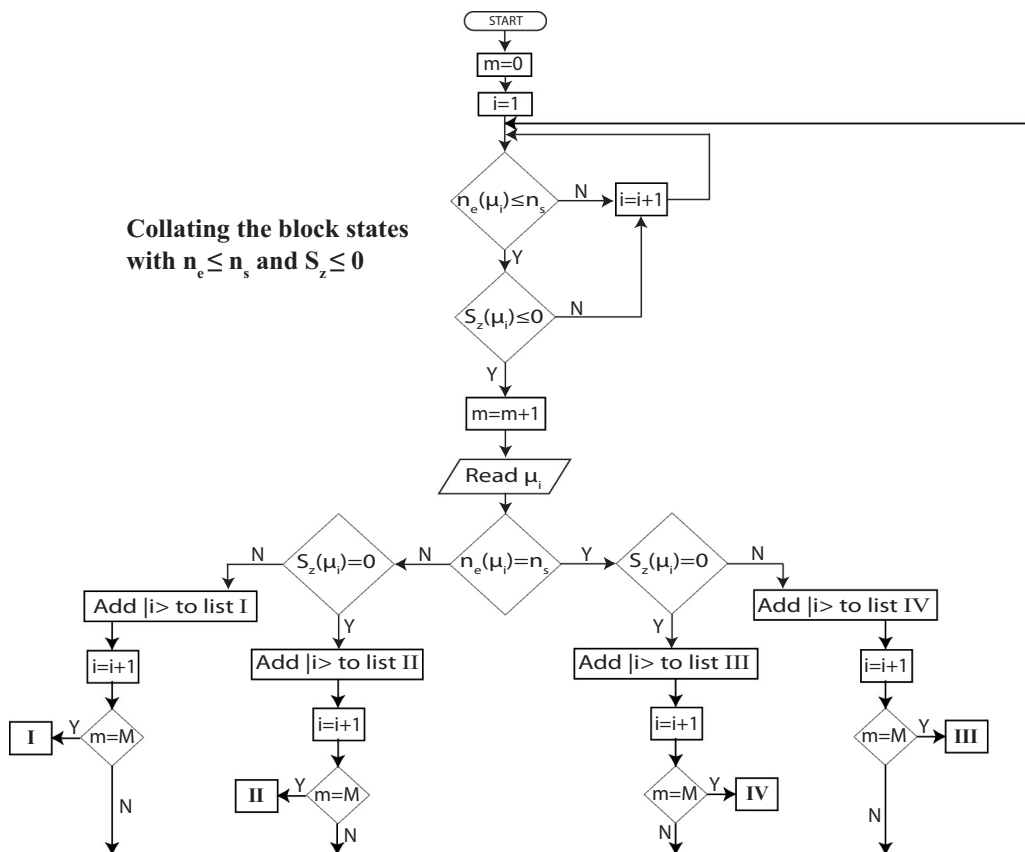


FIG. 1. Schematic flow chart of the modified symmetrized DMRG algorithm. i_I - i_{IV} are the numbers of block states with $\{n_e < n_s, S_z < 0\}$ (list I), $\{n_e < n_s, S_z = 0\}$ (list II), $\{n_e = n_s, S_z < 0\}$ (list III), and $\{n_e = n_s, S_z = 0\}$ (list IV), respectively. μ_i 's are arranged in decreasing order of their eigenvalues. M is the dimension of the truncated block state space which satisfies the condition $n_e \leq n_s$, $S_z \leq 0$. The DMRG cutoff is imposed in this subspace.

in Figs. 1 and 2). We first show how the symmetry operators in a given block can be obtained as sparse matrices with only one nonzero element per each row (or column) in the basis of the block states. There are four distinct cases corresponding to different conditions on n_e and S_z , and we will deal with each of them separately.

(i) $\{\mu_i(\mathbf{n}_e < \mathbf{n}_s, \mathbf{S}_z < \mathbf{0})\}$: Application of J_L, P_L and their product on these block states gives the corresponding symmetry counterparts. As J_L and P_L do not commute in general, we only considered the product $P_L J_L$; the order of operations of the two operators will become irrelevant for the superblock which is a half-filled system, where J and P commute

$$\begin{aligned} \hat{J}_L \mu_i(n_e < n_s, S_z < 0) &= \mu_{i_j}(n_e > n_s, S_z < 0), \\ \hat{P}_L \mu_i(n_e < n_s, S_z < 0) &= \mu_{i_p}(n_e < n_s, S_z > 0), \\ \hat{P}_L \hat{J}_L \mu_i(n_e < n_s, S_z < 0) &= \mu_{i_{p_j}}(n_e > n_s, S_z > 0). \end{aligned} \quad (5)$$

The matrix elements of the symmetry operators in the $\{\mu_i\}$ basis are given by

$$\begin{aligned} (\hat{J}_L)_{i,j} &= (-1)^\eta \delta_{j,i_j}, \quad (\hat{P}_L)_{i,j} = (-1)^\xi \delta_{j,i_p}, \\ (\hat{P}_L \hat{J}_L)_{i,j} &= (-1)^\zeta \delta_{j,i_{p_j}}, \end{aligned} \quad (6)$$

where η , ξ , and ζ are the appropriate phase factors for J , P , and PJ symmetries.

(ii) $\{\mu_i(\mathbf{n}_e < \mathbf{n}_s, \mathbf{S}_z = \mathbf{0})\}$: Application of the J_L symmetry operator on these block states generates block states with

particle number $2n_s - n_e$; yet, P_L symmetry should map the block state space to itself. Therefore, to begin with, this group of block states is further subdivided into smaller subgroups $\{\mu_i(n'_e, S_z = 0)\}$, where n'_e assumes all values of $< n_s$. For each value of n'_e , we set up the matrix of \hat{P} in block states of this subspace. This is diagonalized to obtain the eigenvectors of \hat{P} so that each of the new block states map into itself with a phase factor of ± 1 . These transformed $\tilde{\mu}_i(n'_e, S_z = 0)$'s provide a one-to-one mapping under the symmetry operations \hat{J} , \hat{P} , and $\hat{P}\hat{J}$.

(iii) $\{\mu_i(\mathbf{n}_e = \mathbf{n}_s, \mathbf{S}_z < \mathbf{0})\}$: This set of block states is similar to the one discussed above, differing only in the fact that J_L will map the space to itself instead of P_L . The space is subdivided into smaller blocks on the basis of different negative S_z values, and the matrices of the operator \hat{J} are set up for each S_z value in the block state space. The eigenstates of this operator serve as the new block states for obtaining one-to-one correspondence of the block states under the symmetry operations.

(iv) $\{\mu_i(\mathbf{n}_e = \mathbf{n}_s, \mathbf{S}_z = \mathbf{0})\}$: This particular set of block states spans a vector space which on application by both J_L and P_L should map into itself. Hence, linear combinations which are eigenvectors of J_L with eigenvalues $(-1)^{\zeta_j}$, $\zeta_j = 0$, or 1 are first obtained. Using the eigenvectors of J_L with a particular eigenvalue $(-1)^{\zeta_j}$, another set of linear combinations is formed which are eigenvectors of P_L with eigenvalues $(-1)^{\zeta_p}$, $\zeta_p = 0$, or 1. This is accomplished by first constructing the matrix

Construction of symmetry partners of block states

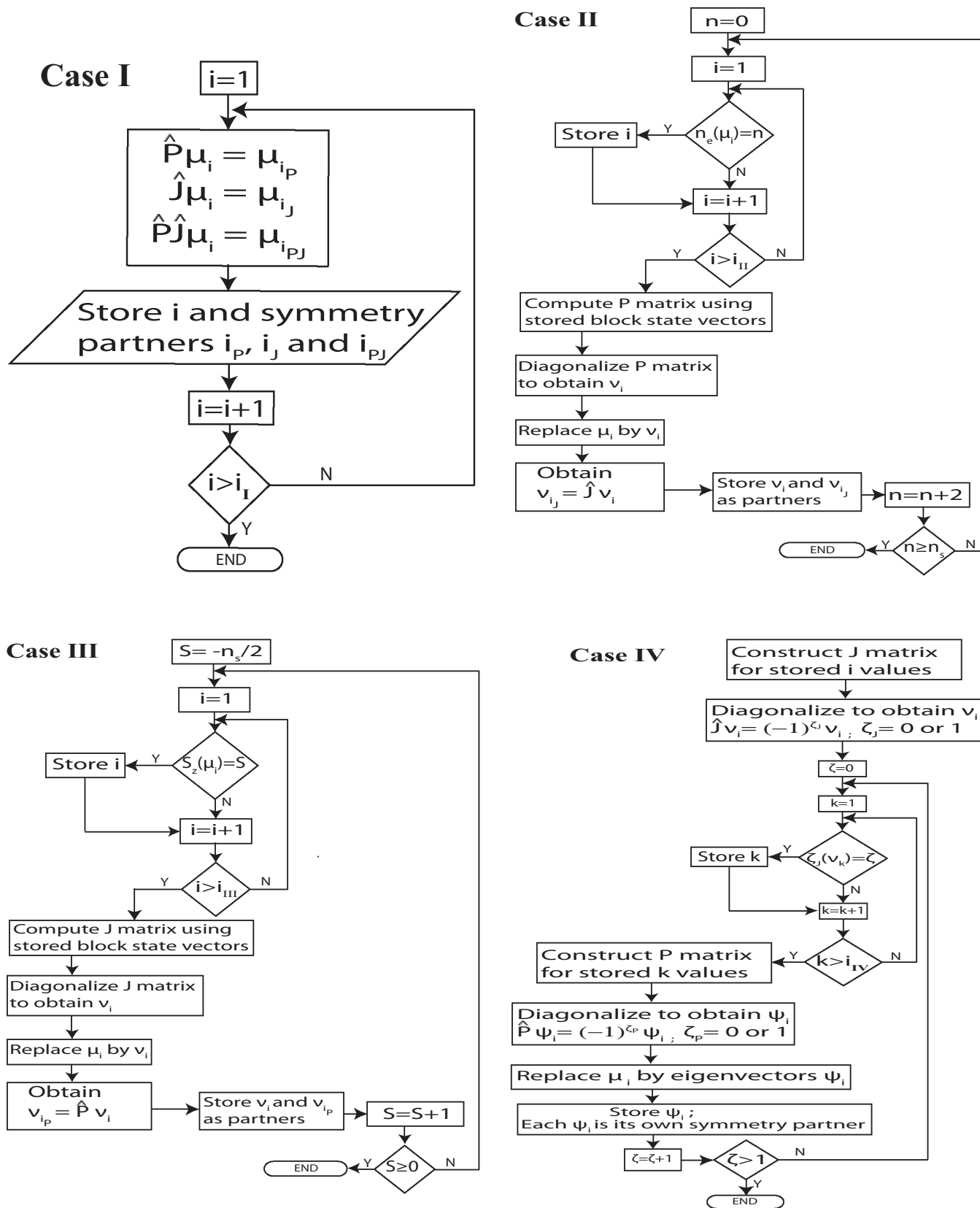


FIG. 2. Continued from Fig. 1 of the previous page.

representation of \hat{J} in the basis of block states with $n_e = n_s$ and $S_z = 0$. We diagonalize the matrix to obtain the eigenvectors of \hat{J} . We then use the eigenvectors of \hat{J} as the basis in which the matrix of \hat{P} is set up. The resulting eigenvectors of \hat{P} replace the block states in this space, and they are employed in symmetry adaptation.

Usually the number of block states we need to retain in the sector, $n_e \leq n_s$ and $S_z \leq 0$, is about $0.4M^{(l)}$, where $M^{(l)}$ is the desired truncation in the block states without any restriction. Since we have a one-to-one correspondence of the block states within a block for the operations \hat{J} , \hat{P} , and $\hat{P}\hat{J}$, it is a simple matter to extend the one-to-one correspondence to the direct product basis states formed by the block states of the left and right blocks and the Fock space states of the newly added sites.

Symmetry adapted direct product bases in an irreducible representation Γ can be generated by employing the projection operator,

$$\hat{P}(\Gamma) = \frac{1}{h} \sum_i \chi(\Gamma, \mathcal{R}_i) \hat{\mathcal{R}}_i, \quad (7)$$

where $\chi(\Gamma, \mathcal{R}_i)$ is the character of the symmetry operator $\hat{\mathcal{R}}_i$ in the irreducible representation Γ and h being the order of the group. Operation by $\hat{P}(\Gamma)$ on each of the basis states in the direct product space produces the symmetry adapted linear combinations. However, if $\hat{P}(\Gamma)$ acts on each of the states in the direct product space, we will end up with a linearly dependent symmetry adapted basis. In the earlier symmetry adaptation procedure [49], weeding out linear dependence by the Gram-Schmidt orthonormalization technique was an extremely expensive step computationally. With the present technique where we have a one-to-one correspondence between symmetry related states, this turns out to be extremely simple and computationally very efficient. First we note that one-to-one correspondence between the DMRG basis states under the symmetry operations implies that a given basis state can appear only once (or not at all) in a given symmetry space. Therefore, in the symmetry adaptation step, we sequentially go through the list of basis states, apply the projection operator, construct the symmetrized combination, and eliminate its partners from the list of unsymmetrized basis states. This ensures that a basis state occurs at most once in the symmetrized states. Taken together with the orthonormality of the unsymmetrized basis states, this also ensures orthogonality of the basis states generated by the projection operator. Using these symmetry combinations, we can generate the transformation matrix S_Γ , which is a $D \times D_\Gamma$ matrix where D is the dimensionality of the unsymmetrized space and D_Γ is the dimensionality of the symmetrized space.

Whereas the symmetrized Hamiltonian in the Γ representation of the augmented system can be constructed by

$$\tilde{H}_{2l+2} = S_\Gamma^\dagger H_{2l+2} S_\Gamma, \quad (8)$$

this operation requires more memory as well as CPU time than the procedure, if we bypass this step, and directly operate with the Hamiltonian on the symmetrized basis states and collate the resulting states into different basis vectors of the symmetry space and collect the matrix elements of the symmetrized Hamiltonian matrix,

$$H|i_\Gamma\rangle_{2l+2} = \sum_k h_{i,k} |k_\Gamma\rangle_{2l+2}. \quad (9)$$

The Hamiltonian is then diagonalized to get lowest-lying eigenvectors in different irreducible representations labeled as ${}^e A^+$, ${}^e B^+$, ${}^e A^-$, ${}^e B^-$, ${}^o A^+$, ${}^o B^+$, ${}^o A^-$, and ${}^o B^-$ where the left superscript represents the character under P symmetry, the right superscript is the character under J symmetry, and the letters A/B denote the character under C_2 symmetry in the irreducible representation Γ . The singlet lies in the e space whereas the triplet lies in the o space. The space $+$ refers to ‘‘covalent’’ space, whereas $-$ refers to the ‘‘ionic’’ space. $A(B)$ represents the space even (odd) under C_2 symmetry. The ground state usually remains in ${}^e A^+$ whereas the optically connected space is ${}^e B^-$. The lowest triplet lies in the ${}^o B^+$ space.

III. COMPARISON WITH EXACT CALCULATION

A. Model Hamiltonian

The model Hamiltonian employed for the current paper is the well-known PPP Hamiltonian [63,64], which considers σ - π separability and incorporates long-range Coulombic interactions along with on-site Hubbard interaction. Numerous studies have revealed that the ground- and excited-state properties in carbon-based π -conjugated systems can be well reproduced within this model Hamiltonian [25,46,65–69].

The PPP Hamiltonian can be written as

$$H = \sum_{(i,j),\sigma} t_0 (\hat{c}_{i,\sigma}^\dagger \hat{c}_{j,\sigma} + \text{H.c.}) + \sum_i \frac{U}{2} \hat{n}_i (\hat{n}_i - 1) + \sum_{i>j} V_{ij} (\hat{n}_i - z_i) (\hat{n}_j - z_j). \quad (10)$$

t_0 is the nearest-neighbor hopping integral between bonded sites i and j whereas U is the on-site Coulomb repulsion term. The intersite interaction energies V_{ij} are interpolated by the Ohno scheme [70,71] assuming a C-C bond length of 1.4 Å. $\hat{c}_{i,\sigma}^\dagger$ and $\hat{c}_{i,\sigma}$ are the creation and annihilation operators of an electron with spin σ in the p_z orbital at site i , and $\hat{n}_i = \sum_\sigma \hat{c}_{i,\sigma}^\dagger \hat{c}_{i,\sigma}$ is the corresponding number operator. For aromatic rings, the nearest-neighbor transfer integral is $t_0 = -2.40$ eV. The Hubbard U for carbon $2p$ orbitals in π conjugation is 11.26 eV which is the sum of the ionization energy and the electron affinity of carbon [72]. z_i is the local chemical potential and corresponds to the number of electrons at site i which leaves the site neutral; for carbon atoms in a π -conjugated system, $z_i = 1$.

B. Results and discussion

The accuracy of our modified algorithm is established by comparing the results obtained for small systems with exact PPP results, such as for a 16-site polyene chain and tetracene molecule which has 18 sites. In Fig. 3, the difference between the ground-state energies of the 16-site polyene chain as obtained by the exact diagonalization technique and by employing the symmetrized DMRG technique are plotted for four different values of the ‘‘number of retained block states’’ in the sector $\{\mu_i^l(n_e \leq n_s, S_z \leq 0)\}(m^{(l)})$. The dimension of the full block space, derived from these $m^{(l)}$ block states employing J and P symmetries is not the same from iteration to iteration; $m^{(l)} = 225$ for polyene chains corresponds to the dimension of the block space in the vicinity of 550 whereas

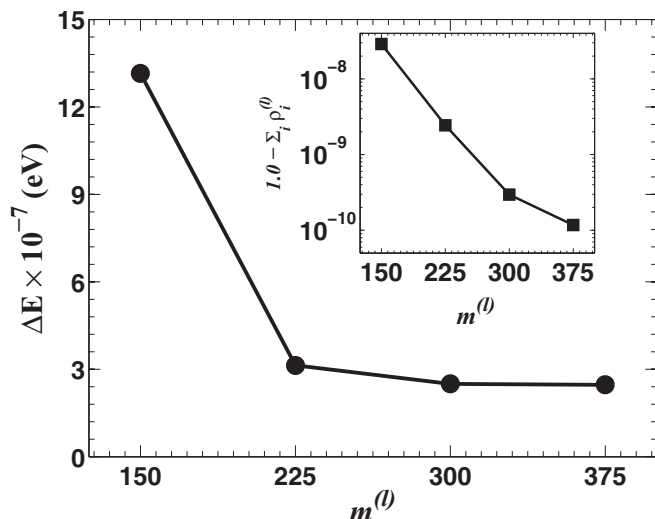


FIG. 3. Deviation of the ground-state energy of a 16-site polyene chain calculated by the symmetrized DMRG technique from the exact energy value for different cutoff $m^{(l)}$'s of the block state space. The number of finite DMRG sweeps (2) is fixed in all the cases. The inset: Truncation error ($1.0 - \sum_i \rho_i^{(l)}$) for different cutoff $m^{(l)}$'s within the symmetrized DMRG calculation for a 16-site polyene chain. The solid lines are given only as a guide to the eye.

$m^{(l)} = 425$ for polyacene molecules results in the block space dimension of ~ 1000 . From Fig. 3, we note that the energy values calculated employing the current SDMRG technique agree within numerical accuracy when compared with exact diagonalization results. We have also plotted the truncation error ($1.0 - \sum_i \rho_i^{(l)}$) corresponding to the final step of the finite DMRG calculation as a function of $m^{(l)}$ (Fig. 3). It can be noted that the truncation error is on the order of 10^{-10} for $m^{(l)} = 375$. In Table II, we have given the difference between the DMRG energy and the exact energy with the number of finite DMRG sweeps for $m^{(l)} = 225$. After the first iteration only, the ground-state energy is accurate to about 10^{-7} eV; therefore two to three sweeps in the finite DMRG calculation will suffice for the desired accuracy.

We have also established the efficiency of the modified algorithm by plotting the computational time required for the generation of the symmetrized DMRG basis states for different $m^{(l)}$'s (Fig. 4). It can be seen that the computational time decreases sublinearly with the increasing cutoff in block states compared with the earlier algorithm.

TABLE II. Fluctuations in the DMRG ground-state energy of a 16-site polyene chain with respect to exact energy with an increasing number of finite DMRG sweeps. The number of block states retained $m^{(l)}$ is 225.

Steps	ΔE_{sweep}
Infinite DMRG	3.62×10^{-5}
Number of sweeps = 1	3.14×10^{-7}
Number of sweeps = 2	3.09×10^{-7}
Number of sweeps = 3	3.13×10^{-7}
Number of sweeps = 4	3.09×10^{-7}

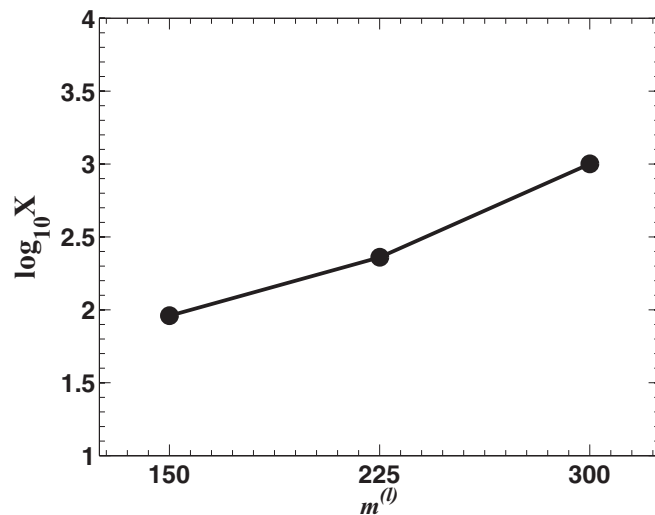


FIG. 4. Variation of computational time required for the generation of the symmetrized DMRG basis states for a 16-site polyene chain within the modified algorithm for different cutoff $m^{(l)}$'s of the block state space. X is the ratio between the computational time required while the Gram-Schmidt orthogonalization is carried out (as in the old algorithm) and while employing the modified algorithm. The solid line is given only as a guide to the eye.

In Table III, PPP energies of the ground-state (1^1A^+), the lowest two-photon state (2^1A^+), the lowest one-photon state (1^1B^-), and of the lowest triplet state (1^3B^+) of both the 16-site polyene chain and the tetracene molecule are presented. Full CI calculations, employing the diagrammatic valence-bond method [73], show excellent agreement with the results obtained and the upper bound of error in energies of different states are on the order of 10^{-4} eV which is negligible compared to experimental accuracies.

IV. APPLICATION TO 1,12-BENZOPERYLENE

We have studied a few low-lying states of 1,12-benzoperylene (Fig. 5) in different symmetry spaces with $m^{(l)} = 400$ which corresponds to the block space of the dimension of ~ 1000 . The model employed is the PPP model, and energy gaps are tabulated in Table IV. We have employed the

TABLE III. Comparison of the energies of the ground state, the lowest two-photon state, the lowest optical state, and the lowest triplet state of the 16-site polyene chain and tetracene, obtained by the modified symmetrized DMRG algorithm and exact calculation. The exact calculations are carried out using the diagrammatic valence-bond method.

System	State	Exact calculation	DMRG calculation
Polyene of 16 sites	1^1A^+	-33.55575	-33.55575
	2^1A^+	-32.03385	-32.03385
	1^1B^-	-30.43291	-30.43291
	1^3B^+	-32.87993	-32.87993
Tetracene molecule	1^1A^+	-43.69083	-43.69076
	2^1A^+	-40.55749	-40.55725
	1^1B^-	-40.51439	-40.51419
	1^3B^+	-42.47046	-42.47038

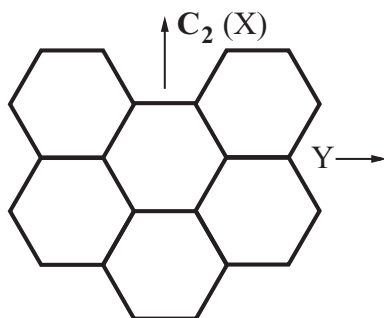


FIG. 5. Schematic of 1,12-benzoperylene. The C_2 axis is taken as the molecular X axis.

C_2 symmetry of the molecule besides electron-hole symmetry and spin-inversion symmetry in the $S_z = 0$ sector. Being treated as a planar molecule, the reflection on the molecular plane is the identity operator and does not correspond to any nontrivial symmetry. We have obtained a few low-lying states in the ${}^eA^+$, ${}^eB^-$, ${}^oB^+$, and ${}^oA^-$ spaces corresponding to the ground-state subspace, the subspace optically connected to the ground state and the odd parity space which includes the triplet subspace. For computing transition dipole moments, average density matrices obtained from the eigenstates of different symmetry subspaces are employed.

The lowest two-photon state is at an energy of 2.99 eV, significantly lower in energy, compared to the lowest optical state. This is in good agreement with experimentally derived values of 2.87–3.10 eV. This state has not been realized by two-photon spectroscopy but has been observed in fluorescence [74,75] and absorption spectroscopy [76,77] as a very weak band. We can attribute this state to the lowest two-photon state

TABLE IV. Low-energy excited states in 1,12-benzoperylene with the energy gaps from the singlet ground state in units of eV. The transition dipole moments from the ground state to the excited states (in debyes) are given in parentheses. For triplets, the transition dipole moments of optical excitations from the lowest triplet state are also given. The transition dipoles in all cases are y polarized.

Nature of the state	State level	Energy gap
Two photon	$2^1A_1^+$	2.99
	$3^1A_1^+$	4.26
	$4^1A_1^+$	4.58
Optical	$1^1B_1^-$	3.72 ^a (3.17)
	$2^1B_1^-$	4.71 ^b (3.83)
	$3^1B_1^-$	4.83 ^b (5.20)
Triplet	$1^3B_1^+$	2.84
	$2^3B_1^+$	3.65
	$3^3B_1^+$	4.26
Triplet optical	$1^3A_1^-$	3.98 (0.46)
	$2^3A_1^-$	5.36 (4.96)
	$3^3A_1^-$	5.61 (1.15)

^aExperimental energy gaps are 3.41 eV [74], 3.22–3.40 eV [75], and 3.35–3.86 eV [76,78,79].

^bExperimental energy gaps are 4.13–4.29 eV [74,75,78,79] and 4.28–4.44 eV [76].

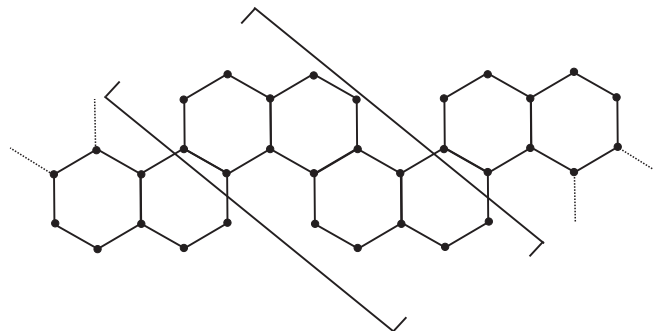


FIG. 6. Schematic of polychrysene. The repeated unit is shown in the parentheses.

because, in real molecules, we do not have strict electron-hole symmetry and the otherwise-forbidden two-photon state acquires some intensity due to symmetry breaking. The three lowest two-photon states have energies of 2.99, 4.26, and 4.58 eV in the covalent space, and none of these states energetically correspond to two triplet states (see Table IV).

The lowest optical gap for vertical transition is 3.72 eV with a transition dipole moment of 3.17 D. There are two other excited states at energies of 4.71 and 4.83 eV, the transition dipole moment to the later being the highest among all three optical states (5.20 D). The total intensity for the transition to states at 4.71 and 4.83 eV is about four times than that for the 3.72-eV state. It is likely that the experimentally observed energy levels in the range of 4.13–4.45 eV (depending upon the solvent) (Refs. [74–76,78,79]) actually correspond to this pair of states. Experimentally, another weak absorption band is also observed between 3.22 and 3.69 eV, which we believe, corresponds to the lowest optically excited state. Our calculated energies correspond to vertical transitions in the gas phase, and the redshift of the peak positions in solvents could be about 0.5 eV resulting in the observed values in solution.

The lowest triplet state energy can be calculated in two ways while employing both C_2 and J symmetries – either by calculating the lowest-energy state in the $S_z = 1$ sector or by

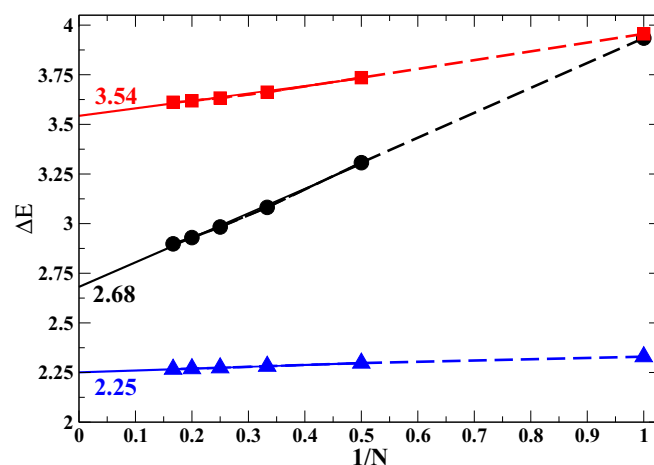


FIG. 7. Lowest one-photon (optical) (■), lowest two-photon (●), and lowest spin gaps (▲) in polychrysene (in units of eV) are plotted as a function of the inverse of the number of chrysene units (N). The extrapolated values of the energy gaps are also shown in the figure.

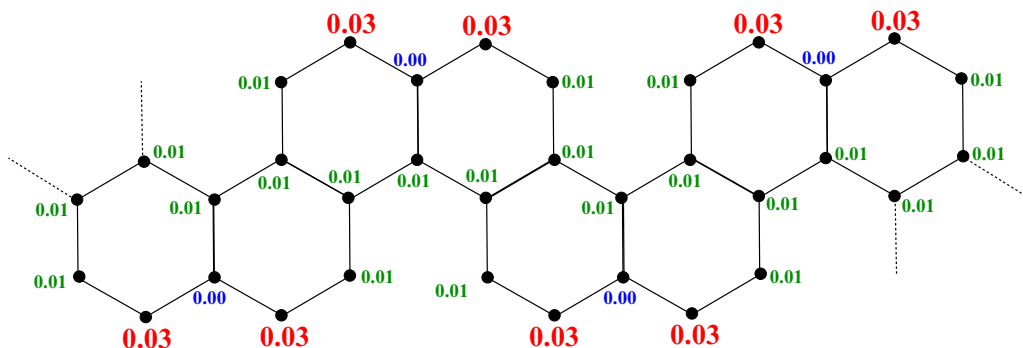


FIG. 8. Site spin densities in the interior part of polychrysene in the lowest triplet state. The spin densities are also color coded—high (red), moderate (dark green), and low (blue).

calculating the lowest-energy state in the $S_z = 0$ space with $\chi_P = -1$ under the spin-inversion symmetry. However, it is numerically more accurate to obtain the triplet state as the lowest $S_z = 1$ state as the effective dimension of the triplet space with $S_z = 0$ and $\chi_P = -1$ is almost half the dimension of the $S_z = 0$ space. Thus, the effective dimension of the triplet space in the $S_z = 1$ subspace is larger than the effective dimension of the triplet space in $S_z = 0$ for $\chi_P = -1$. Since DMRG is a variational technique, the accuracy is higher when the dimension of the space is larger.

The calculated lowest triplet gap in 1,12-benzoperylene is 2.84 eV whereas the experimentally reported lowest triplet gap lies within 2.01–2.02 eV. However, in experiment the triplet energy gaps are deduced via phosphorescence spectroscopy where the system relaxes to the lowest vibrational state of the corresponding triplet surface before radiatively decaying to the ground state. The bond-order calculations (provided in the Supplemental Material [80]) illustrate the considerable structural difference between the ground state and the lowest triplet state. As our calculation considers a rigid molecular structure, we attribute the calculated lowest triplet gap as the vertical gap which could be larger than the measured gap in the phosphorescence study. Based on the relative positions of the lowest optical two-photon and triplet states on the energy scale, we can conclude that 1,12-benzoperylene is a poor candidate for exhibiting singlet fission.

The three lowest triplet states in the ionic subspace are at 3.98, 5.36, and 5.61 eV. The triplet-triplet absorption spectra corresponding to these levels are at 1.14, 2.52, and 2.77 eV whereas the calculated transition matrix elements for these T - T absorptions are 0.46, 4.96, and 1.15 D. Hence, we should observe a strong T - T absorption band around 2.5 eV.

V. APPLICATION TO POLYCHRYSENE

In recent years, graphene nanoribbons have been recognized as potential candidates for nanoscale devices due to their tunable electronic properties. The electronic properties in these systems are primarily determined by their edge structures and their widths. Zigzag and armchair nanoribbons are the most commonly probed systems (Ref. [34] and references therein), whereas in recent years, cove-edge and mixed-edge graphene nanoribbons have also been synthesized by “bottom-up” synthetic approaches [81–86]. Spectroscopic studies as well as theoretical calculations within density functional theory have predicted a finite band gap (~ 2.0 eV) in the cove-edged graphene nanoribbons [81–83]. Presently, we have studied the low-lying electronic structure of a mixed graphene nanoribbon which has both zigzag and cove-edge structures within the PPP model keeping ~ 750 block states. The repeating unit is comprised of a single chrysene molecule and, consequently, we have termed this graphene nanoribbon as polychrysene

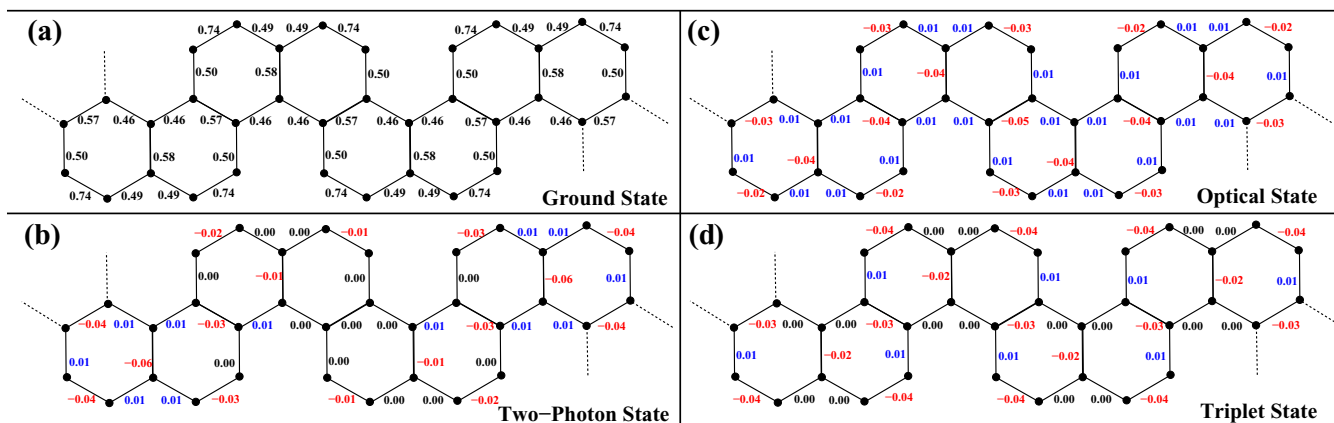


FIG. 9. Bond orders in the interior of polychrysene in (a) the ground state. Differences in bond orders ($b_{ij}^\alpha - b_{ij}^G$) of state α with respect to the ground state in (b) the lowest two-photon state, (c) the lowest optical state, and (d) the lowest triplet state are also shown. The changes are also color coded—positive (blue), zero variation (black), and negative (red).

(Fig. 6). Experimental studies on various cove-edged graphene nanoribbons have revealed distorted nonplanar equilibrium structures [81,82], although in our calculations, we have treated them as planar.

We have studied nanoribbons of varying sizes (N), starting from one to six units, and extrapolated the low-lying excitation gaps to the thermodynamic limit. The lowest optical state remains above the lowest two-photon state for all system sizes, which is a signature of strong effective electronic correlation similar to that in *trans*-polyacetylene (Fig. 7). The lowest optical and two-photon gaps show excellent linear fits with the system size and extrapolate to 3.54 and 2.68 eV, respectively, in the thermodynamic limit. The size dependence of the energy gaps suggests that the optical state has a fairly localized character whereas the two-photon state is more extended over the π -conjugation network. The nonvanishing two-photon gap also signifies that the cove-edge character dominates over the zigzag-edge character since the vanishing two-photon gap has been observed in the narrow zigzag nanoribbon in the thermodynamic limit in an earlier study [34]. We also note that, unlike in linear polyenes and zigzag nanoribbons, the two-photon state does not have the character of two triplets. This is indeed the case in many conjugated systems, such as polyacenes [4] and fused azulenes [87], wherein the conjugation topology is nonlinear. Since the energies of both the one- and the two-photon states are far lower than the energy of the two coupled triplet excitons, these systems will be poor candidates for singlet fission. We have also calculated the transition dipole moment to the lowest optical state for different oligomers and find the transition to be moderately strong (~ 3.0 – 4.0 D), suggesting a moderately strong absorption band for the one-photon state.

The lowest spin gap in these nanoribbons remains almost invariant with system size and extrapolates to 2.25 eV in the thermodynamic limit (Fig. 7). The almost constant spin gap in these nanoribbons gives an impression of highly localized triplet excitons; however, spin densities at different sites (expectation value of $\langle \hat{S}_i^z \rangle$ in the lowest triplet state) indicate the delocalized nature of the exciton, although, the spin densities decrease significantly at the ends of the ribbons (Fig. 8). The spin density is highest in the zigzag segment of the nanoribbons whereas the cove-edge segment has significantly lower spin density.

We have also plotted the bond orders for the ground state and the low-lying excited states of the largest system (Fig. 9). The bond-order patterns are quite similar in all the excited states studied. The bond orders at the ends of the nanoribbons vary slightly from that in the interior section; the bond-order pattern along the zigzag edge corresponds to ($=$ — — $=$), whereas the cove-edge regions have lower bond orders suggesting longer bonds in the cove region. Indeed, this structural feature

has been observed experimentally in cove-edge structured graphene nanoribbons [81,82]. The bond-order patterns also indicate a fairly rigid structure of the graphene nanoribbon and primarily vertical electronic transitions.

VI. CONCLUSION

We have developed a computationally efficient algorithm for symmetry adaptation within the conventional DMRG procedure for conjugated organic molecules. The algorithm introduces a one-to-one symmetry correspondence between basis states leading to extreme sparseness in the symmetry matrices and gets rid of the bottleneck of slow Gram-Schmidt orthonormalization. The efficiency of this algorithm enables us to retain a large number of block states in the DMRG calculations.

We have obtained energy gaps for several one-photon, two-photon, and triplet states in 1,12-benzoperylene within the PPP model employing this algorithm. The PPP model predicts the low-lying excitation energies and transition dipoles quite accurately. The lowest triplet state is nearly degenerate with the lowest two-photon state, and hence singlet fission is not probable. The transition dipole moment to the third one-photon state is the largest among the one-photon states we have calculated. A large spin gap in comparison with polycyclic aromatic hydrocarbons of similar sizes indicates weaker correlation due to greater delocalization of the electrons. On the other hand, the PPP model study of polychrysene exhibits the signature of strong electron correlation in these systems. The cove-edge character dominates over the zigzag-edge features in this mixed graphene nanoribbon whereas the almost system-size-independent spin gap is a distinctive feature. The relative ordering of the low-energy states also suggests that similar to 1,12-benzoperylene, polychrysene is also a poor candidate for singlet fission. It will be interesting to probe the variation in effective electronic correlation strength and relative ordering of energy states with size variation in these polycyclic aromatic hydrocarbons.

ACKNOWLEDGMENTS

We acknowledge Prof. Diptiman Sen for valuable discussions during the development of the modified SDMRG algorithm. We also acknowledge Prof. Sumit Mazumdar for valuable discussions over the course of the study. S.R. is thankful to the Department of Science and Technology (India), India and Indo-U.S. Science and Technology Forum for financial support through a Joint Center, which made this collaboration possible. S.P. acknowledges Council of Scientific & Industrial Research, India for a senior research fellowship. S.P. also thanks Prof. Diptiman Sen for financial support through his J. C. Bose fellowship.

[1] S. R. White, *Phys. Rev. Lett.* **69**, 2863 (1992).

[2] S. R. White, *Phys. Rev. B* **48**, 10345 (1993).

[3] S. Ramasesha, S. K. Pati, Z. Shuai, and J. L. Brédas, in *Advances in Quantum Chemistry*, edited by J. R. Sabin, M. C. Zerner, and E. Brändas (Academic, San Diego, 2000), Vol. 38, pp. 121–215.

[4] C. Raghu, Y. Anusooya Pati, and S. Ramasesha, *Phys. Rev. B* **66**, 035116 (2002).

[5] C. Raghu, Y. Anusooya Pati, and S. Ramasesha, *Phys. Rev. B* **65**, 155204 (2002).

[6] W. Barford and R. J. Bursill, *Chem. Phys. Lett.* **268**, 535 (1997).

[7] W. Barford and R. J. Bursill, *Synth. Met.* **89**, 155 (1997).

[8] M. Boman and R. J. Bursill, *Phys. Rev. B* **57**, 15167 (1998).

[9] R. J. Bursill and W. Barford, *Phys. Rev. Lett.* **82**, 1514 (1999).

- [10] W. Barford, R. J. Bursill, and M. Y. Lavrentiev, *Phys. Rev. B* **63**, 195108 (2001).
- [11] W. Barford, R. J. Bursill, and M. Y. Lavrentiev, *J. Phys.: Condens. Matter* **10**, 6429 (1998).
- [12] M. Y. Lavrentiev, W. Barford, S. J. Martin, H. Daly, and R. J. Bursill, *Phys. Rev. B* **59**, 9987 (1999).
- [13] R. J. Bursill and W. Barford, *Phys. Rev. B* **66**, 205112 (2002).
- [14] W. Barford, R. J. Bursill, and M. Y. Lavrentiev, *Phys. Rev. B* **65**, 075107 (2002).
- [15] W. Barford, R. J. Bursill, and R. W. Smith, *Phys. Rev. B* **66**, 115205 (2002).
- [16] A. Race, W. Barford, and R. J. Bursill, *Phys. Rev. B* **64**, 035208 (2001).
- [17] A. Race, W. Barford, and R. J. Bursill, *Phys. Rev. B* **67**, 245202 (2003).
- [18] R. J. Bursill and W. Barford, *J. Chem. Phys.* **130**, 234302 (2009).
- [19] W. Barford, R. J. Bursill, and D. V. Makhov, *Phys. Rev. B* **81**, 035206 (2010).
- [20] J. Hachmann, J. J. Dorando, M. Avilés, and G. K.-L. Chan, *J. Chem. Phys.* **127**, 134309 (2007).
- [21] D. Ghosh, J. Hachmann, T. Yanai, and G. K.-L. Chan, *J. Chem. Phys.* **128**, 144117 (2008).
- [22] S. Lakshmi, A. Datta, and S. K. Pati, *Phys. Rev. B* **72**, 045131 (2005).
- [23] W. Mizukami, Y. Kurashige, and T. Yanai, *J. Chem. Theory Comput.* **9**, 401 (2013).
- [24] B. S. Hudson, B. E. Kohler, and K. Schulten, in *Excited States*, edited by E. C. Lim (Academic, New York, 1982), Vol. 6, p. 1.
- [25] Z. G. Soos and S. Ramasesha, *Phys. Rev. B* **29**, 5410 (1984).
- [26] K. Tandon, S. Ramasesha, and S. Mazumdar, *Phys. Rev. B* **67**, 045109 (2003).
- [27] Z. Shuai, D. Beljonne, R. J. Silbey, and J. L. Brédas, *Phys. Rev. Lett.* **84**, 131 (2000).
- [28] H. Zhao and S. Mazumdar, *Phys. Rev. Lett.* **93**, 157402 (2004).
- [29] C. D. Spataru, S. Ismail-Beigi, L. X. Benedict, and S. G. Louie, *Phys. Rev. Lett.* **92**, 077402 (2004).
- [30] E. Chang, G. Bussi, A. Ruini, and E. Molinari, *Phys. Rev. Lett.* **92**, 196401 (2004).
- [31] S. Dutta and S. K. Pati, *J. Phys. Chem. B* **112**, 1333 (2008).
- [32] K. Aryanpour, A. Roberts, A. Sandhu, R. Rathore, A. Shukla, and S. Mazumdar, *J. Phys. Chem. C* **118**, 3331 (2014).
- [33] K. Aryanpour, A. Shukla, and S. Mazumdar, *J. Chem. Phys.* **140**, 104301 (2014).
- [34] V. M. L. Durga Prasad Goli, S. Prodhana, S. Mazumdar, and S. Ramasesha, *Phys. Rev. B* **94**, 035139 (2016).
- [35] T. Yamamoto, T. Noguchi, and K. Watanabe, *Phys. Rev. B* **74**, 121409 (2006).
- [36] B. M. Wong, *J. Phys. Chem. C* **113**, 21921 (2009).
- [37] G. Mallocci, G. Cappellini, G. Mulas, and A. Mattoni, *Chem. Phys.* **384**, 19 (2011).
- [38] L. Yang, J. Deslippe, C.-H. Park, M. L. Cohen, and S. G. Louie, *Phys. Rev. Lett.* **103**, 186802 (2009).
- [39] Y.-W. Son, M. L. Cohen, and S. G. Louie, *Phys. Rev. Lett.* **97**, 216803 (2006).
- [40] Y.-W. Son, M. L. Cohen, and S. G. Louie, *Nature (London)* **444**, 347 (2006).
- [41] M. Schreiber, M. R. Silva-Junior, S. P. A. Sauer, and W. Thiel, *J. Chem. Phys.* **128**, 134110 (2008).
- [42] M. R. Silva-Junior, M. Schreiber, S. P. A. Sauer, and W. Thiel, *J. Chem. Phys.* **133**, 174318 (2010).
- [43] J. H. Starcke, M. Wormit, J. Schirmer, and A. Dreuw, *Chem. Phys.* **329**, 39 (2006).
- [44] S. Knippenberg, D. R. Rehn, M. Wormit, J. H. Starcke, I. L. Ruskova, A. B. Trofimov, and A. Dreuw, *J. Chem. Phys.* **136**, 064107 (2012).
- [45] C. M. Krauter, M. Pernpointner, and A. Dreuw, *J. Chem. Phys.* **138**, 044107 (2013).
- [46] P. Tavan and K. Schulten, *J. Chem. Phys.* **85**, 6602 (1986).
- [47] U. Schollwöck, *Rev. Mod. Phys.* **77**, 259 (2005).
- [48] K. A. Hallberg, *Adv. Phys.* **55**, 477 (2006).
- [49] S. Ramasesha, S. K. Pati, H. R. Krishnamurthy, Z. Shuai, and J. L. Brédas, *Phys. Rev. B* **54**, 7598 (1996).
- [50] S. Prodhana, S. Mazumdar, and S. Ramasesha (to be published).
- [51] D. Zgid and M. Nooijen, *J. Chem. Phys.* **128**, 014107 (2008).
- [52] S. Sharma and G. K.-L. Chan, *J. Chem. Phys.* **136**, 124121 (2012).
- [53] S. Wouters, W. Poelmans, P. W. Ayers, and D. Van Neck, *Comput. Phys. Commun.* **185**, 1501 (2014).
- [54] R. Mitsunashi, Y. Suzuki, Y. Yamanari, H. Mitamura, T. Kambe, N. Ikeda, H. Okamoto, A. Fujiwara, M. Yamaji, N. Kawasaki, Y. Maniwa, and Y. Kubozono, *Nature (London)* **464**, 76 (2010).
- [55] Y. Kubozono, H. Mitamura, X. Lee, X. He, Y. Yamanari, Y. Takahashi, Y. Suzuki, Y. Kaji, R. Eguchi, K. Akaike, T. Kambe, H. Okamoto, A. Fujiwara, T. Kato, T. Kosugi, and H. Aoki, *Phys. Chem. Chem. Phys.* **13**, 16476 (2011).
- [56] I. P. McCulloch and M. Gulácsi, *Aust. J. Phys.* **53**, 597 (2000).
- [57] I. P. McCulloch and M. Gulácsi, *Philos. Mag. Lett.* **81**, 447 (2001).
- [58] I. P. McCulloch and M. Gulácsi, *Europhys. Lett.* **57**, 852 (2002).
- [59] J. Dukelsky and S. Pittel, *Rep. Prog. Phys.* **67**, 513 (2004).
- [60] M. Tinkham, *Group Theory and Quantum Mechanics* (Dover, New York, 2003).
- [61] G. Barcza, O. Legeza, F. Gebhard, and R. M. Noack, *Phys. Rev. B* **81**, 045103 (2010).
- [62] G. Barcza, W. Barford, F. Gebhard, and O. Legeza, *Phys. Rev. B* **87**, 245116 (2013).
- [63] R. Pariser and R. G. Parr, *J. Chem. Phys.* **21**, 466 (1953).
- [64] J. A. Pople, *Trans. Faraday Soc.* **49**, 1375 (1953).
- [65] P. Tavan and K. Schulten, *J. Chem. Phys.* **70**, 5407 (1979).
- [66] P. Tavan and K. Schulten, *J. Chem. Phys.* **70**, 5414 (1979).
- [67] P. Tavan and K. Schulten, *Phys. Rev. B* **36**, 4337 (1987).
- [68] Z. G. Soos, S. Ramasesha, and D. S. Galvao, *Phys. Rev. Lett.* **71**, 1609 (1993).
- [69] D. Baeriswyl, D. K. Campbell, and S. Mazumdar, in *Conjugated Conducting Polymers*, edited by H. Kiess, Springer Series in Solid-State Sciences Vol. 102 (Springer, Berlin, 1992).
- [70] K. Ohno, *Theor. Chim. Acta* **2**, 219 (1964).
- [71] G. Klopman, *J. Am. Chem. Soc.* **86**, 4550 (1964).
- [72] L. Salem, *The Molecular Orbital Theory of Conjugated Systems* (W. A. Benjamin, Reading, MA, 1966), p. 420.
- [73] S. Ramasesha and Z. Soos, *Int. J. Quan. Chem.* **25**, 1003 (1984).
- [74] R. Dabestani and I. N. Ivanov, *Photochemistry and Photobiology* **70**, 10 (1999).
- [75] S. Hirayama, H. Sakai, Y. Araki, M. Tanaka, M. Imakawa, T. Wada, T. Takenobu, and T. Hasobe, *Chem. Eur. J.* **20**, 9081 (2014).
- [76] J. Aihara, K. Ohno, and H. Inokuchi, *Bull. Chem. Soc. Jpn.* **43**, 2435 (1970).
- [77] O. Birer, P. Moreschini, and K. K. Lehmann, *Phys. Chem. Chem. Phys.* **10**, 1648 (2008).

- [78] E. Clar, *Polycyclic Hydrocarbons* (Springer-Verlag, Berlin/Heidelberg, 1964), Vol. 2.
- [79] E. Clar and W. Schmidt, *Tetrahedron* **33**, 2093 (1977).
- [80] See Supplemental Material at <http://link.aps.org/supplemental/10.1103/PhysRevB.97.195125> for the bond-order values of 1,12-benzoperylene in the ground state, the lowest two-photon state, the lowest optical state, and the lowest triplet state. A schematic of 1,12-benzoperylene with the bond indices is also provided in the Supplemental Material.
- [81] J. Liu, B.-W. Li, Y.-Z. Tan, A. Giannakopoulos, C. Sanchez-Sanchez, D. Beljonne, P. Ruffieux, R. Fasel, X. Feng, and K. Müllen, *J. Am. Chem. Soc.* **137**, 6097 (2015).
- [82] T. J. Sisto, Y. Zhong, B. Zhang, M. Tuan Trinh, K. Miyata, X. Zhong, X.-Y. Zhu, M. L. Steigerwald, F. Ng, and C. Nuckolls, *J. Am. Chem. Soc.* **139**, 5648 (2017).
- [83] M. Daigle, D. Miao, A. Lucotti, M. Tommasini, and J.-F. Morin, *Angew. Chem.* **129**, 6309 (2017).
- [84] Y. Zhong, B. Kumar, S. Oh, M. Tuan Trinh, Y. Wu, K. Elbert, P. Li, X. Zhu, S. Xiao, F. Ng, M. L. Steigerwald, and C. Nuckolls, *J. Am. Chem. Soc.* **136**, 8122 (2014).
- [85] J. Ma, J. Liu, M. Baumgarten, Y. Fu, Y.-Z. Tan, K. S. Schellhammer, F. Ortman, G. Cuniberti, H. Komber, R. Berger, K. Müllen, and X. Feng, *Angew. Chem. Int. Ed.* **56**, 3280 (2017).
- [86] K. Xu, Y. Fu, Y. Zhou, F. Hennersdorf, P. Machata, I. Vincon, J. J. Weigand, A. A. Popov, R. Berger, and X. Feng, *Angew. Chem. Int. Ed.* **56**, 15876 (2017).
- [87] S. Thomas, S. Ramasesha, K. Hallberg, and D. Garcia, *Phys. Rev. B* **86**, 180403 (2012).